J Mol Model (2015) 21: 26
DOI 10.1007/s00894-015-2581-9

ORIGINAL PAPER

Theoretical study of the stabilities and detonation performance of 5-nitro-3-trinitromethyl-1*H*-1,2,4-triazole and its derivatives

Xueli Zhang · Xuedong Gong

Received: 5 November 2014 / Accepted: 7 January 2015 / Published online: 29 January 2015
© Springer-Verlag Berlin Heidelberg 2015

Abstract 5-Nitro-3-trinitromethyl-1*H*-1,2,4-triazole (NTMT, A) and its substituted derivatives A–CH_3, A–OCH_3, A–NH_2, A–OH, A–NO_2, and A–ONO_2 were studied using density functional theory (DFT). For all of the molecules except for A–ONO_2, the C–NO_2 bond in the trinitromethyl group was found to be the weakest, and no transition state occurred during the scission of this bond. The weakest C–NO_2 of the trinitromethyl group bond dissociation energies for all of the molecules were all very similar. Most of the title molecules had similar frontier orbital distributions and comparable energy gaps between the frontier orbitals. The impact sensitivity (h_{50}, in cm), predicted at various levels of theory, decreased in the order A–NH_2 (53.0–71.0)>A–CH_3 (53.0)>A (36.7)>A–OCH_3 (32.6–42.3)>A–OH (26.7–53.0)>A–NO_2 (5.6–7.4)>A–ONO_2 (4.6–6.1). Their detonation velocities (D), detonation pressures (P), and specific impulses (I_s) were 8.02–8.82 km/s, 29.92–35.54 GPa, and 214–260 s, respectively. Composite explosives made from hexahydro-1,3,5-trinitro-1,3,5-triazine (RDX) and A, A–OH, A–NH_2, A–NO_2, or A–ONO_2 as an oxidizer were found to possess much better detonation performance (D=9.04–9.29 km/s, P=37.25–39.26 GPa, and I_s=270–281 s). Thus, introducing –OCH_3, –OH, and –NH_2 groups into A produced new explosives with acceptable stability and good detonation performance. A–OH and A–NH_2 appear to be promising candidates for oxidizers in composite explosives.

Keywords Triazole derivatives · Stability · Detonation performance · Density functional theory

Electronic supplementary material The online version of this article (doi:10.1007/s00894-015-2581-9) contains supplementary material, which is available to authorized users.

X. Zhang · X. Gong (✉)
School of Chemical Engineering, Nanjing University of Science and Technology, Nanjing 210094, China
e-mail: gongxd325@mail.njust.edu.cn

Introduction

Energetic materials attract great attention because of their wide range of military and industrial applications [1–4]. A multitude of explosives have been prepared in order to meet the various requirements for energetic materials. 1,3,5,7-Tetranitro-1,3,5,7-tetraazacyclooctane (HMX), 1,3,5-trinitro-1,3,5-triazacyclohexane (RDX), 2,4,6-trinitrotoluene (TNT), nitroglycerin (NG), and nitrocellulose (NC) [5–10] are the most commonly used and famous classical explosives. New explosives such as hexaazahexanitroisowurtzitane (CL-20), 2,6-diamino-3,5-dinitropyrazine-1-oxide (LLM-105), 1,1-diamino-2,2-dinitroethylene (FOX-7), and 1,3,3-trinitroazetidine (TNAZ) have also been applied in military and civilian arenas [10–19]. The requirements of energetic materials—low sensitivity, high energy, and high oxygen balance (OB)—have resulted in a continuous search for new explosives. Polynitroazoles are the new stars in the field of energetic materials due to their high detonation performance and low sensitivities to friction and impact [20–25]. A variety of powerful nitroazoles have been prepared [26–31]. During ongoing efforts to find more powerful, less sensitive, and eco-friendly energetic nitroazole explosives, Shreeve's team found a new molecule: 5-nitro-3-trinitromethyl-1*H*-1,2,4-triazole (NTMT, A in Fig. 1) [32]. This is a heterocyclic compound with high oxygen (48.7 %) and nitrogen (37.3 %) contents and low carbon (13.6 %) and hydrogen (0.4 %) contents, which results in a positive OB (9.2 %). NTMT has a high heat of formation (HOF, 123.2 kJ/mol^{-1}), which is helpful for improving detonation performance. Its positive OB, high HOF, environmentally benign decomposition products, and acceptable thermal stability (decomposition temperature T_d=135 °C) and impact sensitivity (h_{50}=36.7 cm, 2.5 kg drop hammer) [32] indicate that NTMT may be a potential candidate for an oxidizer.

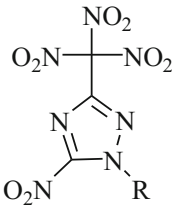

A	R=H	OB= 9.1
A-CH_3	R=CH_3	OB= -8.7
A-OCH_3	R=OCH_3	OB= -2.7
A-NH_2	R=NH_2	OB= 5.8
A-OH	R=OH	OB= 14.3
A-NO_2	R=NO_2	OB= 20.8
A-ONO_2	R=ONO_2	OB= 24.7

Fig. 1 Structures of A and its derivatives

A substituted derivative of NTMT, 5-trinitro-3-trinitromethyl-1-methyl-1,2,4-triazole (NTMMT, A–CH_3), has also been prepared by mixing A with trimethylsilyl diazomethane [32]. A–CH_3 has good thermal stability (T_d= 153 °C) and impact sensitivity (h_{50}=53.0 cm), a high HOF (95.6 kJ/mol^{-1}), and appealing detonation properties [32]. These attractive properties of A and A–CH_3 inspired us to search for new derivatives of NTMT with other functional groups, i.e., –OCH_3, –NH_2, –OH, –NO_2, and –ONO_2 (see Fig. 1). In order to assess the potential of these new derivatives as explosives, we predicted their thermal stabilities, impact sensitivities, chemical stabilities, and detonation properties in the solid state, as reported in this paper.

Computational details

Geometry optimizations for all compounds were performed at the M06-2X/6-311++G**, B3LYP/6-31G*, and B3PW91/6-31G** levels of theory using the Gaussian software package [33]. All geometries were verified to be the local energy minima via frequency analysis. Relaxed potential energy surface scans were carried out and the stretching of C–NO_2 in the trinitromethyl group C–C(NO_2)$_3$ and in C(R)–NO_2 (i.e., the C in the C–NO_2 group is in the ring) in all molecules, the stretching of N–NO_2 in A–NO_2, and the stretching of O–NO_2 in A–ONO_2 were investigated at the B3LYP/6-31G* level.

The bond dissociation energy (BDE), which is key to elucidating the mechanism of pyrolysis and thermal stability [34–37], was calculated at the M06-2X/6-311++G**, B3LYP/6-31G*, and B3PW91/6-31G** levels using the following equation:

$$\mathrm{BDE} = E_{\mathrm{R1}\cdot} + E_{\mathrm{R2}\cdot} - E_{\mathrm{R1—R2}}, \quad (1)$$

where $E_{\mathrm{R1—R2}}$, $E_{\mathrm{R1}\cdot}$, and $E_{\mathrm{R2}\cdot}$ are the zero-point-corrected total energies of the parent molecule and the radicals produced by bond scission, respectively.

Q_{Nitro} is the algebraic sum of charges on the atoms in a nitro group, obtained using

$$Q_{\mathrm{Nitro}} = Q_{\mathrm{N}} + Q_{\mathrm{O1}} + Q_{\mathrm{O2}\cdot} \quad (2)$$

The average value of Q_{Nitro} ($\overline{Q}_{\mathrm{Nitro}}$) was calculated using

$$\overline{Q}_{\mathrm{Nitro}} = \frac{1}{n}\sum_{i=1}^{n} Q_{\mathrm{Nitro},i}, \quad (3)$$

where n is the number of nitro groups in the molecule of interest.

The electrostatic potential $V(r)$ created by the nuclei and electrons of a molecule in its environment was obtained using

$$V(r) = \sum_{A} \frac{Z_A}{|R_A - r|} - \int \frac{\rho(r')dr'}{|r' - r|}. \quad (4)$$

Here, Z_A is the charge on nucleus A located at R_A, and $\rho(r)$ is the electronic density.

σ_+^2, σ_-^2, and σ_{tot}^2 are the positive, negative, and total variances of the surface electrostatic potential at r ($V_s(r)$). These reflect the range or variability of $V_s(r)$ and were obtained using the following equations:

$$\sigma_+^2 = \frac{1}{n}\sum_{i=1}^{n}\left[V_{\mathrm{S}}^{+}(r_i) - V_{\mathrm{S,ave}}^{+}\right]^2 \quad (5)$$

$$\sigma_-^2 = \frac{1}{m}\sum_{j=1}^{m}\left[V_{\mathrm{S}}^{-}(r_j) - V_{\mathrm{S,ave}}^{-}\right]^2 \quad (6)$$

$$\sigma_{\mathrm{tot}}^2 = \sigma_+^2 + \sigma_-^2. \quad (7)$$

Here, i and j are the indices of the sampling points in positive and negative regions, respectively. n and m are the number of positive and negative points on the surface, respectively. $V_{\mathrm{S}}^{+}(r_i)$ and $V_{\mathrm{S}}^{-}(r_j)$ are the electrostatic potentials at points i and j. $V_{\mathrm{S,ave}}^{+}$ and $V_{\mathrm{S,ave}}^{-}$ denote the average positive and negative electronic potentials on the surface, respectively.

v indicates the degree of balance between the positive and negative electrostatic potentials:

$$v = \frac{\sigma_+^2\sigma_-^2}{(\sigma_{\mathrm{tot}}^2)^2}. \quad (8)$$

The density was calculated using the equation below, in which the intermolecular interactions were taken into

account via the electrostatic interactions on the molecular surface [38]:

$$\rho = \alpha_1 \frac{M}{V(0.001)} + \beta_1 \nu \sigma_{\text{tot}}^2 + \gamma_1. \quad (9)$$

Here, M is the molecular mass in g/mol. $V(0.001)$ is the volume that is encompassed by the 0.001-au contour of the molecule's electronic density. Geometry optimizations and calculations of electrostatic parameters were performed at the B3PW91/6-31G** level of theory. The values of the coefficients α_1, β_1, and γ_1 were taken from [38].

The isodesmic reaction method was employed to predict the gas-phase HOFs ($\Delta_f H(g)$) of the title compounds:

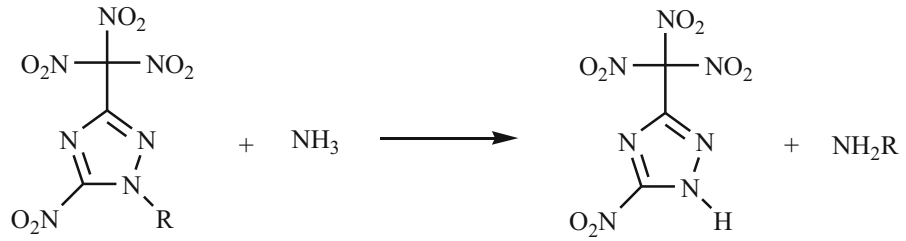

(10)

The enthalpy of reaction ($\Delta_r H_{298}$) at 298 K for this isodesmic reaction was calculated using the following equation:

$$\begin{aligned} \Delta_r H_{298} &= \sum \Delta_f H_P - \sum \Delta_f H_R \\ &= \Delta E_0 + \Delta E_{zpv} + \Delta H_T + \Delta nRT \end{aligned}, \quad (11)$$

where $\Delta_f H_P$ and $\Delta_f H_R$ are the HOFs of the products and the reactants, respectively. ΔE_0 is the difference in total energy between the products and the reactants at 0 K. The MP2/6-311++G**//B3LYP/6-31G* level of theory was employed in this work to predict ΔE_0 more accurately. ΔE_{zpv} is the difference in zero-point energy (E_{zpv}) between the products and the reactants, and ΔH_T is the thermal correction from 0 K to 298 K, which were both calculated at the B3LYP/6-31G* level. ΔnRT is the work term, which equals zero here. Since the HOFs of A, NH_3, NH_2NH_2, and CH_3NH_2 are available [32, 39], the HOFs of the others (NH_2OCH_3, NH_2OH, NH_2NO_2, and NH_2ONO_2) were estimated using the atomization reaction method at the G3 level.

The HOF in the solid state ($\Delta_f H(s)$) was estimated using the following equation:

$$\Delta_f H(s) = \Delta_f H(g) - \Delta_{sub} H. \quad (12)$$

Here, $\Delta_{sub} H$ is the enthalpy of sublimation estimated using the equation below, as suggested by Rice and Politzer et al. [40, 41]:

$$\Delta_{sub} H = \alpha_2 A_s^2 + \beta_2 \left(\nu \sigma_{\text{tot}}^2\right)^{0.5} + \gamma_2. \quad (13)$$

In this equation, A_s is the surface area of the 0.001-au isosurface of the electron density, and ν and σ_{tot}^2 were obtained at the B3LYP/6-31G* level of theory. The values of the coefficients α_2, β_2, and γ_2 were taken from [40].

Detonation velocity (D) and detonation pressure (P), which are important properties of energetic materials,

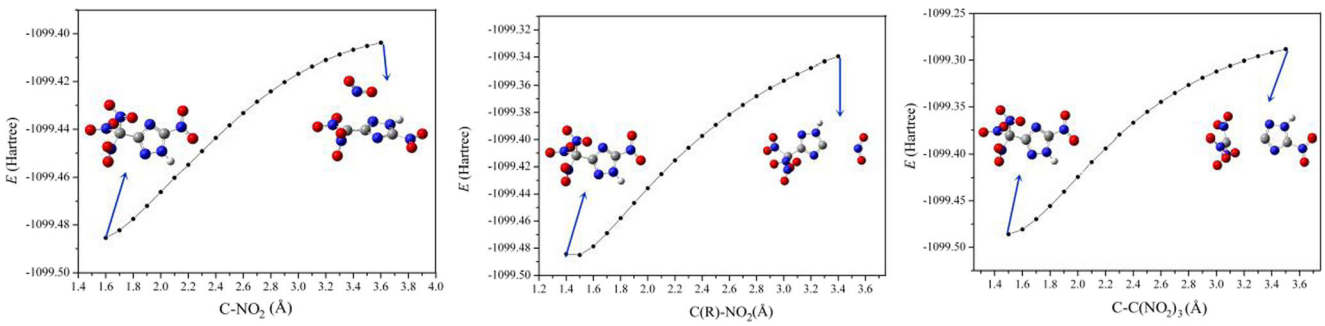

Fig. 2 Plots showing how the energy changes as the lengths of the C–NO_2, C(R)–NO_2, and C–$C(NO_2)_3$ bonds in A are varied

Table 1 Predicted BDEs (in kJ/mol) of the bonds C–NO_2, C(R)–NO_2, and C–$C(NO_2)_3$, calculated at various levels of theory[a]

	M06-2X			B3LYP			B3PW91		
	C–NO_2	C(R)–NO_2	C–$C(NO_2)_3$	C–NO_2	C(R)–NO_2	C–$C(NO_2)_3$	C–NO_2	C(R)–NO_2	C–$C(NO_2)_3$
A	164.0	282.1	465.6	110.1	266.4	409.8	115.5	270.6	412.7
A–CH_3	163.1	280.7	469.5	109.2	261.9	412.8	114.6	266.7	415.9
A–OCH_3	162.3	275.7	466.1	108.5	257.3	408.6	113.8	260.4	411.9
A–NH_2	159.7	272.5	468.4	105.1	260.3	412.2	110.3	264.9	415.4
A–OH	160.0	266.2	448.1	110.1	266.4	409.8	110.7	257.1	411.4
A–NO_2	162.8	249.0	455.5	105.4	253.2	408.1	113.6	234.4	404.6
A–ONO_2	162.5	273.5	458.5	108.4	231.1	401.6	113.3	256.2	405.9

[a] The BDE of the N–NO_2 bond in A–NO_2 was 169.0, 376.7, and 142.1 kJ/mol when calculated at the M06-2X/6-311++G**, B3LYP/6-31G*, and B3PW91/6-31G** levels of theory, and that of the O–NO_2 bond in A–ONO_2 was 86.3, 65.9, and 69.4 kJ/mol when calculated at those levels, respectively

were estimated via the empirical Kamlet–Jacobs equations [42] as follows:

$$D = 1.01\left(N^{0.5}M_{ave}{}^{0.25}Q^{0.25}\right)(1 + 1.30\rho) \quad (14)$$

$$P = 1.558\rho^2 N \; M_{ave}{}^{0.5}Q^{0.5}. \quad (15)$$

Here, N is the number of moles of gaseous detonation products per gram of explosives, M_{ave} is the mean molecular mass of the detonation products, and Q is the detonation energy (cal/g). N, M_{ave}, and Q are determined based on the maximum exothermicity principle [42].

The specific impulse (I_s) was calculated with a widely adopted method [43] using the following equation:

$$I_s = kT_C{}^{0.5}N^{0.5}. \quad (16)$$

k (19.26) was determined via the experimentally evaluated I_s value of CL-20, and this constant was then used to accurately reproduce the I_s values of TNAZ (1,3,3-trinitroazetidine) and RDX (hexahydro-1,3,5-trinitro-1,3,5-triazine). T_C is the temperature in the combustion chamber, calculated using

$$-\Delta H_c = C_{p,g}(T_C - T_0), \quad (17)$$

where ΔH_c represents the enthalpy of combustion and $C_{p,g}$ is the total heat capacity of the gaseous products. T_0 is the initial temperature.

Results and discussion

Bond stability

Bond stability is a conventional index that reflects the thermal stability of explosives [35–37, 44–48]. To evaluate the thermal stabilities of the title molecules, the stabilities of several bonds of A and its derivatives were predicted. These included the weakest C–NO_2 bond in the trinitromethyl group, the C(R)–NO_2 bond (i.e., where the C atom is in the ring), the C–$C(NO_2)_3$ bond, the N–NO_2 bond for A–NO_2, and the O–NO_2 bond for A–ONO_2. Since the bond-breaking processes for the weakest C–NO_2 of trinitromethyl group, C(R)–NO_2, and C–$C(NO_2)_3$ bonds of the derivatives are similar to those of A, only those of A are shown in Fig. 2. The simulated processes of N–NO_2 and O–NO_2 bond dissociation are also similar to those presented in Fig. 2.

Figure 2 shows that the energy of A increases as the weakest C–NO_2 bond of the trinitromethyl group, C(R)–NO_2, and C–$C(NO_2)_3$ bonds lengthen, the slopes of the curves gradually decrease, and the energy ultimately

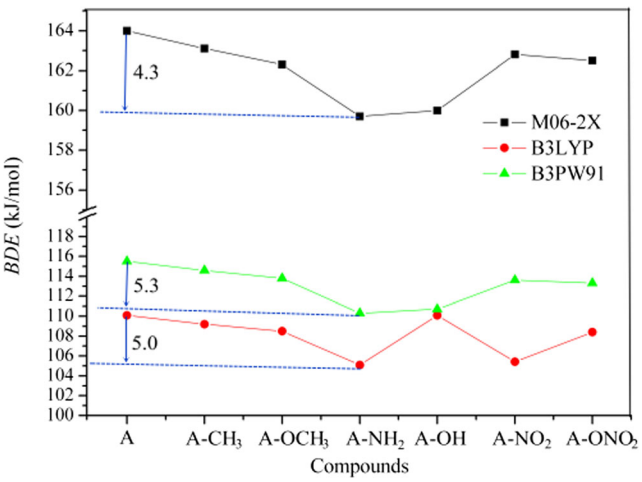

Fig. 3 Variation in the BDE of the weakest C–NO_2 bond of the trinitromethyl group, as calculated at various levels of theory

Table 2 Predicted $\overline{Q}_{Nitro}$ values and h_{50} values of the title molecules, calculated at three levels of theory

Compound	M06-2X		MP2		B3PW91	
	$\overline{Q}_{Nitro}$ (*e*)	h_{50} (cm)	$\overline{Q}_{Nitro}$ (*e*)	h_{50} (cm)	$\overline{Q}_{Nitro}$ (*e*)	h_{50} (cm)
A	−0.140	36.7 [32]	−0.168	36.7 [32]	−0.119	36.7 [32]
A–CH_3	−0.145	53.0 [32]	−0.172	53.0 [32]	−0.123	53.0 [32]
A–OCH_3	−0.139	34.6	−0.166	32.6	−0.121	42.3
A–NH_2	−0.147	64.4	−0.172	53.0	−0.125	71.0
A–OH	−0.145	53.0	−0.163	27.0	−0.115	26.7
A–NO_2	−0.076	7.4	−0.101	6.3	−0.056	5.6
A–ONO_2	−0.058	6.1	−0.083	5.1	−0.040	4.6

plateaus. This behavior reveals that transition states (TSs) do not occur during the dissociation processes for these bonds, and the products are two radicals. Therefore, the required energies for these processes are the differences between the total energies of the radical products and the reactant (i.e., the BDEs). Different methods (M06-2X/6-311++G**, B3LYP/6-31G*, and B3PW91/6-31G**) were employed to evaluate the BDE, and the results obtained are listed in Table 1. The three levels of theory applied provided the same results: the weakest C–NO_2 bonds of the trinitromethyl group were found to have significantly smaller BDEs than the C(R)–NO_2 and C–$C(NO_2)_3$ bonds did, so breaking the former bonds should be much easier than breaking the C(R)–NO_2 and C–$C(NO_2)_3$ bonds. The BDE of the N–NO_2 bond is larger than that of the weakest C–NO_2 bond of the trinitromethyl group in A–NO_2, so the former is stronger than the latter. For A–ONO_2, the BDE of the O–NO_2 bond is significantly smaller than that of the weakest C–NO_2 of the trinitromethyl group, i.e., scission of the O–NO_2 bond should be the initial step in the decomposition of A–ONO_2. In conclusion, the weakest C–NO_2 bond of the trinitromethyl group is the weakest bond, so it breaks first in all of the molecules aside from A–ONO_2.

As shown in Fig. 3, the BDE of the weakest C–NO_2 bond of the trinitromethly group decreases in the order A>A–CH_3>A–OCH_3>A–NO_2>A–OH>A–NH_2. It is noteworthy that the maximum differences in BDE (ΔBDE=BDE(A) – BDE(A–NH_2)) in Fig. 3 are 4.3, 5.0, and 5.2 kJ/mol^{-1} when calculated at the M06-2X/6-311++G**, B3LYP/6-31G*, and B3PW91/6-31G** levels of theory, respectively. This indicates that the weakest C–NO_2 bond of A is slightly weakened by the introduction of substituents. This conclusion further implies that the other derivatives in which the weakest bond is the weakest C–NO_2 bond in the trinitromethyl group may also have BDEs of the weakest C–NO_2 of the trinitromethyl group that are similar to that of A.

The BDE of the weakest C–NO_2 bond of the trinitromethyl group was 159.7–164.0, 105.1–110.1, and 110.3–115.5 kJ/mol^{-1} when calculated at the M06-2X/6-311++G**, B3LYP/6-31G*, and B3PW91/6-31G** levels of theory, so the B3LYP/6-31G* level yields the smallest values. BDEs obtained at the M06-2X/6-311++G** level are considerably larger than those obtained at the other levels of theory. To identify the most reliable results, the BDEs of the C–NO_2 bonds of nitrobenzene, 4-aminonitrobenzene, and 1,3-ditrinitrobenzene (all of which have experimentally available BDE values) were calculated at the three levels of theory. The results are listed in Table S1 of the "Electronic supplementary material" (ESM). The BDEs obtained at the B3LYP/6-31G* and B3PW91/6-311G** levels were smaller than the corresponding experimental BDEs, while those obtained at the M06-2X/6-311++G** level were bigger. The average deviation of the computed BDE from the experimental one was smallest for the results obtained at the B3LYP/6-31G* level (−6.8 kJ/mol^{-1}), rather than the M06-2X/6-311++G** (14.9 kJ/mol^{-1}) and B3PW91/6-31G** (−13.3 kJ/mol^{-1}) levels. Therefore, the results computed at the B3LYP/6-31G* level of theory should be the most reliable.

Impact sensitivity

A continuing major concern in the area of energetic materials is their tendency to explode due to external stimuli. Impact sensitivity is the degree of vulnerability of an energetic material to an external impact. It is widely used to reflect the stability of explosives, and is commonly measured via the parameter h_{50}. The

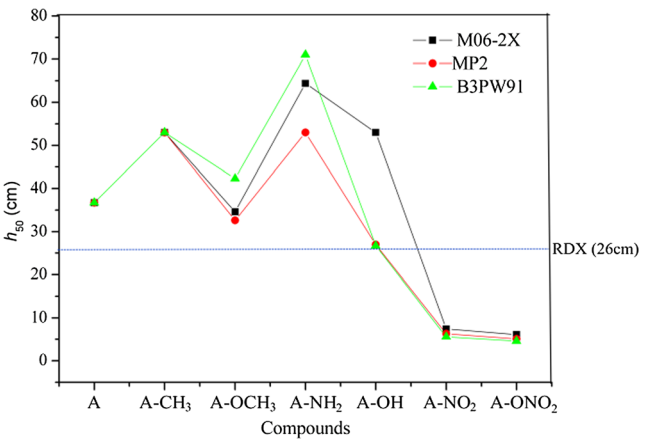

Fig. 4 h_{50} values of A and its derivatives, obtained at three levels of theory

Table 3 Predicted σ_+^2, σ_-^2, ν, and $V_{s,max}$ values of the three C–NO_2 bonds in the trinitromethyl group

Compound	σ_+^2 (kJ/mol)^2	σ_-^2 (kJ/mol)^2	ν	$V_{s,max}(1)$ (kJ/mol)	$V_{s,max}(2)$ (kJ/mol)	$V_{s,max}(3)$ (kJ/mol)
A	5089.1	264.3	0.047	118.0	120.5	97.5
A–CH_3	2506.9	362.4	0.110	106.3	112.1	81.6
A–OCH_3	2146.3	316.9	0.112	114.2	118.0	87.0
A–NH_2	4593.7	329.1	0.062	108.8	120.1	84.1
A–OH	5071.6	367.6	0.063	125.1	145.6	87.9
A–NO_2	2524.4	157.6	0.055	138.5	141.8	124.7
A–ONO_2	1787.4	213.6	0.095	128.9	131.8	108.4

smaller the value of h_{50}, the higher the impact sensitivity. In order to assess the impact sensitivities of A and its derivatives, the nitro group charge method (NGCM) [19]—which makes use of the roughly linear relation between the reciprocal of impact sensitivity $\left(\frac{1}{h_{50}}\right)$ and $\overline{Q}_{Nitro}$, and has been used in some investigations [32, 49]—was applied to predict the h_{50} values of the title molecules. Thus, $\overline{Q}_{Nitro}$ values were calculated (Table 2) at the M06-2X/6-311++G**, MP2/6-311++G**, and B3PW91/6-31G** levels of theory. Since the structures of the title molecules are similar, a strong linear relationship between their $\frac{1}{h_{50}}$ values and their $\overline{Q}_{Nitro}$ values was expected. The experimental h_{50} values of A and A–CH_3 are available [32]. Three linear equations linking the $\overline{Q}_{Nitro}$ values obtained at the three levels of theory with the $\frac{1}{h_{50}}$ values of A and A–CH_3 were fitted to allow the h_{50} values of the other molecules to be predicted:

$$\mathrm{M06{-}2X}: \quad \frac{1}{h_{50}} = 0.26189 + 1.67601\overline{Q}_{Nitro}$$

$$\mathrm{B3PW91}: \quad \frac{1}{h_{50}} = 0.31217 + 2.39427\overline{Q}_{Nitro}$$

$$\mathrm{MP2}: \quad \frac{1}{h_{50}} = 0.5801 + 1.97177\overline{Q}_{Nitro}.$$

The predicted h_{50} values are listed in Table 2 and depicted graphically in Fig. 4. Although the calculated $\overline{Q}_{Nitro}$ values vary depending on the level of theory applied, the predicted h_{50} values show similar variations among the derivatives of A whatever the level of theory used; the deviations between the values obtained at the three levels are not significant. A–NH_2 possesses the lowest impact sensitivity (53.0–71.0 cm). A–NO_2 and A–ONO_2 are the most sensitive of the derivatives: their h_{50} values are about 4.6–7.4 cm. The h_{50} value of A–OCH_3 (32.6–42.3) is comparable to that of A (36.7 cm). Generally speaking, the impact sensitivities of all the molecules aside from A–NO_2 and A–ONO_2 were found to be lower than that of RDX (26 cm) [30], a widely used explosive, meaning that their impact sensitivities are acceptable. The very positive Q_{Nitro} values of the extra –NO_2 groups in A–NO_2 and A–ONO_2 result in less negative $\overline{Q}_{Nitro}$ values, which evidently make A–NO_2 and A–ONO_2 more attractive to electrons and further increase their impact sensitivities.

Surface electrostatic potentials

Murray [50] and Politzer et al [51] pointed out that, for the C–NO_2 bond, a more positive $V_{s,max}$ (the positive extreme of the surface electrostatic potential) value usually corresponds to a smaller bond dissociation energy, and the most sensitive molecules generally have higher anomalous charge imbalances. To assess the relative sensitivities of the title molecules, the positive and negative variances (σ_+^2 and σ_-^2) and the ν and $V_{s,max}$ values of the three C–NO_2 bonds of the trinitromethyl

Table 4 Predicted E_{HOMO}, E_{LUMO}, and E_g values (all in eV) of A and its derivatives, and contributions of the substituents in these molecules to their frontier orbitals (in %)[a]

Compound	E_{HOMO} M06-2X	E_{LUMO} M06-2X	E_g M06-2X	E_g MP2	E_g B3PW91	P_{HOMO}	P_{LUMO}
A	−11.25	−3.00	8.25	12.44	5.50		
A–CH_3	−10.86	−2.75	8.11	12.27	5.46	3.5	0.7
A–OCH_3	−10.93	−2.74	8.19	12.48	5.42	6.2	0.9
A–NH_2	−10.21	−2.80	7.41	11.71	4.79	41.9	2.2
A–OH	−10.89	−2.76	8.13	12.43	5.38	18.8	1.2
A–NO_2	−11.57	−3.42	8.15	12.71	5.19	2.6	49.4
A–ONO_2	−11.30	−3.25	8.05	12.37	5.30	9.8	8.2

[a] P_{HOMO} and P_{LUMO} are the contributions of the substituents to the HOMO and LUMO, respectively

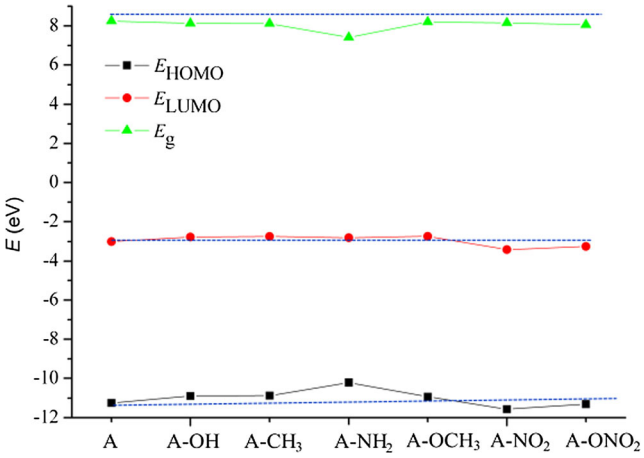

Fig. 5 Trends in E_{HOMO}, E_{LUMO}, and E_g among the title compounds, as calculated at the M06-2X/6-311++G** level

group were evaluated at the B3PW91/6-31G(d,p)//B3PW91/6-31++G(3d,2p) level used in the literature [51], and the results are listed in Table 3. As is evident from this table, σ_+^2 is far larger than σ_-^2, which shows that the strength and variability of the positive surface potential are stronger and larger than those of the negative surface potentials, which agrees well with the characteristics of energetic compounds. The ν values of the derivatives are closer to 0.25 than they are to A, reflecting the idea that the introduction of functional groups onto A helps to improve the balance between the positive and negative surface potentials. The maximum $V_{s,max}$ value among the three C–NO_2 bonds in each title molecule decreases in the order A–OH>A–NO_2>A–ONO_2>A>A–NH_2>A–OCH_3>A–CH_3. Although this order is not exactly the same as the order of C–NO_2 bond BDEs among these molecules, or the order of predicted h_{50} values among them, the order of molecules is very similar for all three parameters, meaning that $V_{s,max}$ is a good indicator of the relative sensitivities of the title molecules. In addition, the $V_{s,max}$ values of A–NO_2 are larger than those of A, i.e., the introduction of the extra –NO_2 group weakens the original C–NO_2 bonds and lowers their BDEs, which is reflected in the smaller BDE of the C–NO_2 bond of A–NO_2 in comparison with that of A.

Chemical stability

The energy gap (E_g) between the frontier orbitals is a widely used parameter that reflects the stability of a molecule to chemical or photochemical processes involving electron transitions or jumps [52, 53]. The E_g values of A and its derivatives were calculated at the three levels of theory and the results are tabulated in Table 4. The E_g values of all of the molecules except for A–NH_2 were similar whichever level of theory was used, which means that the chemical stabilities of the derivatives are comparable to that of A. In other words, introducing a functional group (aside from an –NH_2 group) onto A barely affects its chemical stability.

It is clear that A–NH_2 presents far smaller E_g values than the other compounds. Why is this? Figure 5 shows that the E_{HOMO} values and E_{LUMO} values of A–OH, A–CH_3, A–OCH_3, and A–ONO_2 are very similar to those of A, which leads to similar E_g values too. The E_{HOMO} and E_{LUMO} values of A–NO_2 are lower than those of A, and the drop in E_{LUMO} is slightly larger than the drop in E_{HOMO} with respect to A. For A–NH_2, E_{LUMO} is comparable to that of A, but its E_{HOMO} is much higher than that of A, which leads to its smaller E_g.

The frontier orbital distributions were computed to determine their effects on E_{HOMO} and E_{LUMO}. Since A, A–CH_3, A–

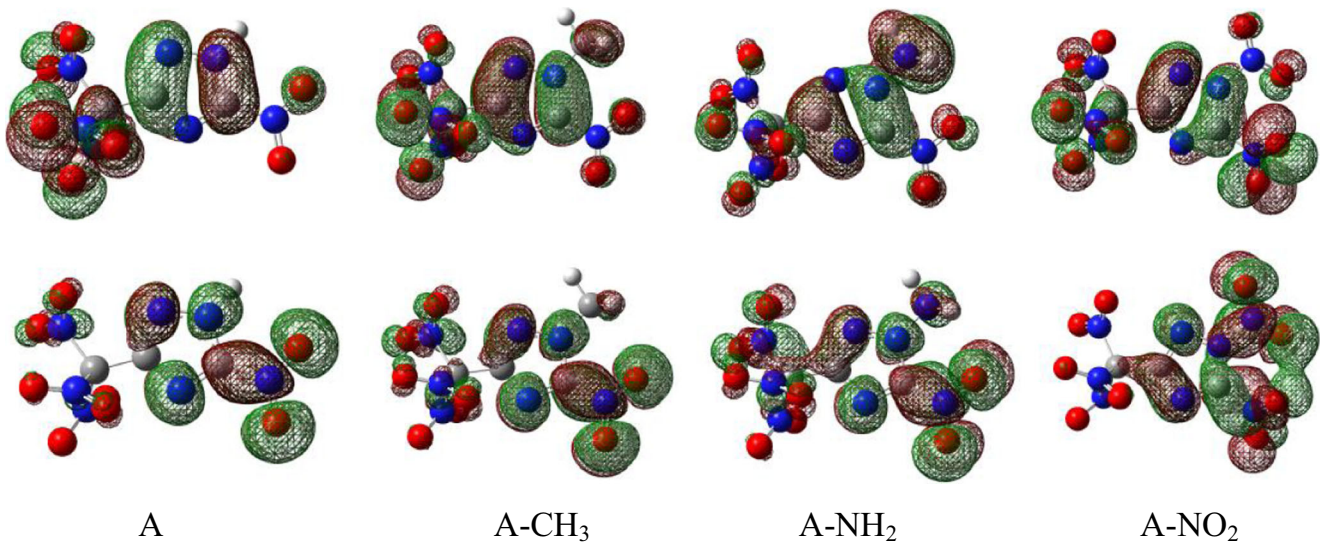

Fig. 6 HOMOs (*top*) and LUMOs (*bottom*) of A, A–CH_3, A–NH_2, and A–NO_2

OCH_3, A–OH, and A–ONO_2 show similar HOMO and LUMO distributions, only those of A and A–CH_3 are shown in Fig. 6, along with the HOMOs and LUMOs of A–NH_2 and A–NO_2. The percentage contributions of the substituents to the HOMO and LUMO were evaluated using the Multiwfn program [54], and the results are listed in Table 4. The HOMOs of A and A–CH_3 are mainly located at the C–N bonds in the triazole ring and the O atoms in the trinitromethyl group, while the LUMOs are mainly associated with the three N atoms in the ring and the C(R)–NO_2 group. The –CH_3 group makes minor contributions to the HOMO and LUMO (3.5 % and 0.7 %). The similar HOMO and LUMO distributions for A and A–CH_3 result in similar E_{HOMO} values, E_{LUMO} values, and E_g values for these molecules, and the same is true of A–OCH_3, A–OH, and A–ONO_2. For A–NH_2, the –NH_2 group makes a considerable contribution (41.9 %) to the HOMO, causing a significant increase in E_{HOMO}. The LUMO is barely affected by the introduction of the –NH_2 group, so the E_{LUMO} of A–NH_2 is close to that of A. The LUMO distribution of A–NO_2 and the contribution of the –NO_2 group (49.4 %) to it both show that the –NO_2 group considerably affects the LUMO distribution, which may be responsible for the smaller E_{LUMO} of A–NO_2 than A.

Detonation properties

The energy content of an energetic molecule can be gauged from its heat of formation, which is an important parameter of energetic materials. In this paper, the gas-phase HOFs (Δ_fH(g) values) of A and its derivatives were predicted by the isodesmic reaction method. The results listed in Table 5 show that the Δ_fH(g) values are 114.7–298.2 kJ/mol^{-1}. The fact that the Δ_fH(g) values are highly positive reveals that these molecules store a large amount of heat, which improves their detonation properties. As a matter of fact, most explosives exist in the solid state under normal conditions, so solid HOFs (Δ_fH(s) values) are required to be able to evaluate the detonation performance of solid molecules. In order to obtain Δ_fH(s) values, we determined the ΔH_{sub} values of the title molecules (cf. Table 6). The data in Table 6 show that all of the molecules except for A–CH_3 have positive Δ_fH(s) values, which aid detonation performance.

Detonation velocity, detonation pressure, and specific impulse are the most important detonation characteristics of energetic materials, and Q and ρ are the most influential factors in these detonation characteristics. The predicted Q, ρ, D, P, and I_s values are shown in Table 7. We see that introducing a –CH_3, –OCH_3, or –NH_2 group decreases the density of A, while introducing a –OH, –NO_2, or –ONO_2 group increases it. Only the addition of –OCH_3 or –NH_2 helps to improve Q and I_s. The solid detonation properties of A–OCH_3, A–NH_2, and A–OH are better than those of A, due to their larger Q and ρ values. The D values (8.59–8.82 km/s) and P values (33.72–35.54 GPa) of A, A–OCH_3, A–NH_2, and A–OH are comparable to or larger than those of RDX (D=8.75 km/s and P= 34.00 GPa), so these molecules can be used as single compound explosives.

A plot of Q versus oxygen balance (OB) (see Fig. 7) shows that Q initially increases but then decreases with increasing OB, and it achieves its maximum value when OB equals −2.72, which the closest plotted OB value to zero. As the absolute value of OB shifts further away from zero, Q gets smaller and smaller. The excess O atoms in molecules (i.e., explosives) with positive OB values are converted into O_2 molecules during explosions, and these O_2 molecules extract some of the heat from the explosion, which results in smaller Q values for the explosives. When the OB of the explosive is negative, some of the C and H atoms are not oxidized during

Table 5 The total energy (E_0), zero-point energy (E_{ZPV}), thermal correction (H_T), and heat of formation in the gas phase (Δ_fH(g)) for various compounds[a]

Compound	E_0 (au)	E_{ZPV} (kJ/mol)	H_T (kJ/mol)	Δ_fH(g) (kJ/mol)
NH_3	−56.21367	90.7	10.0	−46.1 [58]
NH_2CH_3	−95.24502	169.2	11.5	−23.5 [39]
NH_2OCH_3	−170.06232	180.1	14.3	−23.6
NH_2NH_2	−111.20838	139.7	11.9	93.4 [39]
NH_2OH	−131.03021	105.8	11.0	−39.1
NH_2NO_2	−259.69604	101.1	11.5	9.1
NH_2ONO_2	−334.49760	111.8	16.0	44.0
A	−1093.89241	252.6	43.4	123.2 [32]
A–CH_3	−1132.93492	326.3	47.8	114.7
A–OCH_3	−1207.73532	335.3	50.8	157.3
A–NH_2	−1148.89529	295.9	47.1	237.5
A–OH	−1168.69335	259.7	47.4	166.2
A–NO_2	−1297.33212	253.6	51.3	287.3
A–ONO_2	−1372.14217	264.3	53.8	298.2

[a] Δ_fH(g) values of NH_3 derivatives (except for those indicated) were calculated using the atomization method

Table 6 Calculated enthalpy of sublimation ($\Delta_{sub}H$) and heat of formation in the solid (Δ_fH(s)) for each of the title compounds

Compound	A_s (Å^2)	σ^2 (kJ/mol)^2	ν	$\Delta_{sub}H$ (kJ/mol)	Δ_fH(s) (kJ/mol)
A	222.08773	5253.7	0.04791	23.9	23.1
A–CH_3	240.78091	2848.6	0.11072	28.8	−5.6
A–OCH_3	252.85216	2485.4	0.11363	30.7	28.9
A–NH_2	234.95037	4855.6	0.06339	27.5	122.6
A–OH	231.58095	5356.3	0.06365	27.4	51.8
A–NO_2	250.40602	2834.1	0.05800	27.7	171.3
A–ONO_2	261.72042	2053.3	0.09363	30.8	169.2

Table 7 Detonation properties of the title molecules

Compound	ρ (g/cm^3)	Q (cal/g)	D (km/s)	P (GPa)	I_s (s)
A	1.91	1203.7	8.59	33.85	246.1
A–CH_3	1.84	1156.9	8.22	30.34	237.2
A–OCH_3	1.83	1398.6	8.67	33.72	260.5
A–NH_2	1.89	1328.2	8.82	35.54	258.4
A–OH	1.94	1159.3	8.62	34.43	242.5
A–NO_2	1.93	1047.5	8.35	32.23	232.8
A–ONO_2	1.95	870.9	8.02	29.92	214.0

Table 8 Detonation properties of composite explosives that include A or derivatives of it

Composite	w / w	ρ (g/cm^3)	Q (cal/g)	D (km/s)	P (GPa)	I_s (s)
RDX/A	0.70/0.30	1.88	1480.7	9.04	37.25	270.0
RDX/A–OH	0.60/0.40	1.89	1574.6	9.25	39.04	280.1
RDX/A–NH_2	0.79/0.21	1.88	1498.2	9.10	37.68	272.4
RDX/A–NO_2	0.51/0.49	1.88	1551.4	9.19	38.47	277.9
RDX/A–ONO_2	0.47/0.53	1.88	1604.1	9.29	39.26	280.7

the explosion, so maximum heat release is impossible, leading to a smaller Q value. On the whole, the smaller the absolute value of OB, the higher the Q value.

The presence of excess oxygen atoms lowers the detonation performance of A, A–OH, A–NH_2, A–NO_2, and A–ONO_2 when they are used as single compound explosives, but they can be fully utilized in composite explosives as oxidizers. Our previous studies [55, 56] showed that composite explosives containing both oxygen-rich explosives and oxygen-poor explosives present enhanced detonation performance. Thus, composite explosives of RDX using A, A–OH, A–NH_2, A–NO_2, and A–ONO_2 as oxidizers were studied. The weight ratios of these composite explosives were adjusted to make the OBs of the mixtures zero. The explosive reactions of these composite explosives are as follows:

A / RDX	2C3HO8N7 (s) + C3H6N6O6 (s) = 9CO2 (g) + 4H2O (g) + 10N2 (g)
A-OH/RDX	6C3HO9N7 (s) + 5C3H6N6O6 (s) = 33CO2 (g) + 18H2O (g) + 36N2 (g)
A-NH2/RDX	3C3H2O8N8(s) + C3H6N6O6 (s) = 12CO2 (g) + 6H2O (g) + 15N2 (g)
A-NO2/RDX	3C3O10N8 (s) + 4C3H6N6O6 (s) = 21CO2 (g) + 12H2O (g) + 24N2 (g)
A-ONO2/RDX	3C3HO8N7 (s) + 5C3H6N6O6 (s) = 24CO2 (g) + 15H2O (g) + 27N2 (g)

The calculated detonation properties of these mixtures are tabulated in Table 8. The densities of these mixtures are 1.88–1.89 g/cm^3, which are between those of the corresponding oxidizer and RDX. The Q values of these composite explosives are far larger than those of their components when they are used as single compound explosives. These considerable improvements in Q can be attributed to the full utilization of the excess oxygen present in the oxidizers, which means that no heat is lost to the excess oxygen of the oxidizers and full oxidization of the carbon and hydrogen atoms in RDX occurs, releasing more heat. The D values and P values of these mixtures are 9.04–9.29 km/s and 37.25–39.26 GPa, respectively. The detonation performance of each composite explosive is obviously better than those of its components, and is comparable to that of HMX. The I_s values of these mixtures are close to or even better than that of CL-20 (278.8 s) [57].

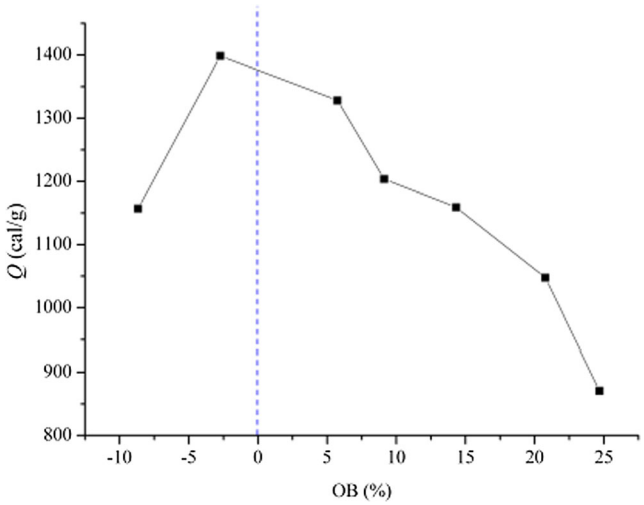

Fig. 7 Plot of Q versus oxygen balance (OB)

Conclusions

The C–NO_2 bond of the trinitromethyl group is the weakest bond in A, A–CH_3, A–OCH_3, A–NH_2, A–OH, and A–NO_2, and no TS occurs during the decomposition of this bond. The BDEs of the weakest C–NO_2 bonds of the trinitromethyl group in these molecules are very similar, whatever the level of theory used to calculate them. The contributions of –CH_3, –OCH_3, –OH, and –ONO_2 to the HOMO and LUMO distributions are small, meaning that their E_g values are comparable to

that of A. The impact sensitivities of A, A–CH_3, A–OCH_3, A–NH_2, and A–OH are acceptable (26.7–71 cm), while those of A–NO_2 and A–ONO_2 are quite high (4.6–7.4 cm).

The D, P, and I_s values of A and its derivatives are 8.02–8.82 km/s, 29.92–35.54 GPa, and 214–260 s, respectively. A, A–OCH_3, A–NH_2, and A–OH show moderately good detonation performance when used as single compound explosives. Composite explosives containing RDX and A, A–OH, A–NH_2, A–NO_2, or A–ONO_2 as an oxidizer have much better detonation properties (D=9.04–9.29 km/s, P=37.25–39.26 GPa, and I_s=270–281 s) than those of A or its derivatives.

References

1. Rahm M, Brinck T (2010) Kinetic stability and propellant performance of green energetic materials. Chem Eur J 16(22):6590–6600
2. Klapötke TM, Krumm B, Moll R, Rest SF (2011) CHNO based molecules containing 2,2,2-trinitroethoxy moieties as possible high energy dense oxidizers. Z Anorg Allg Chem 637(14–15):2103–2110
3. Badgujar DM, Talawar MB, Asthana SN, Mahulikar PP (2008) Advances in science and technology of modern energetic materials: an overview. J Hazard Mater 151(2):289–305
4. Sikder A, Sikder N (2004) A review of advanced high performance, insensitive and thermally stable energetic materials emerging for military and space applications. J Hazard Mater 112(1):1–15
5. Urbanski T (1964) Chemistry and technology of explosives, vol 6. Pergamon, New York
6. Agrawal JP (1998) Recent trends in high-energy materials. Prog Energ Combust 24(1):1–30
7. Singh G, Kapoor IPS, Mannan SM, Kaur J (2000) Studies on energetic compounds. Part 8: Thermolysis of Salts of HNO_3 and $HClO_4$. J Hazard Mater 79(1):1–18
8. Fried LE, Manaa MR, Pagoria PF, Simpson RL (2001) Design and synthesis of energetic materials 1. Ann Rev Mater Res 31(1):291–321
9. Shlyapochnikov V, Tafipolsky M, Tokmakov I, Baskir E, Anikin O, Strelenko YA, Luk'yanov O, Tartakovsky V (2001) On the structure and spectra of dinitramide salts. J Mol Struct 559(1):147–166
10. Pagoria PF, Lee GS, Mitchell AR, Schmidt RD (2002) A review of energetic materials synthesis. Thermochim Acta 384(1):187–204
11. An C, Li H, Geng X, Li J, Wang J (2013) Preparation and properties of 2,6-diamino-3,5-dinitropyrazine-1-oxide based nanocomposites. Propell Explos Pyrot 38(2):172–175
12. Zhang J, Wu P, Yang Z, Gao B, Zhang J, Wang P, Nie F, Liao L (2014) Preparation and properties of submicrometer-sized LLM-105 via spray-crystallization method. Propell Explos Pyrot 39(5):653–657
13. Bolton O, Simke LR, Pagoria PF, Matzger AJ (2012) High power explosive with good sensitivity: a 2:1 cocrystal of CL-20: HMX. Cryst Growth Des 12(9):4311–4314
14. Bayat Y, Zeynali V (2011) Preparation and characterization of nano-CL-20 explosive. J Energ Mater 29(4):281–291
15. Mandal AK, Thanigaivelan U, Pandey RK, Asthana S, Khomane RB, Kulkarni BD (2012) Preparation of spherical particles of 1,1-diamino-2,2-dinitroethene (FOX-7) using a micellar nanoreactor. Org Process Res Dev 16(11):1711–1716
16. Vo TT, Zhang J, Parrish DA, Twamley B, Shreeve JM (2013) New roles for 1,1-diamino-2,2-dinitroethene (FOX-7): halogenated FOX-7 and azo-bis (diahaloFOX) as energetic materials and oxidizers. J Am Chem Soc 135(32):11787–11790
17. Behrens R Jr, Bulusu S (2013) Thermal decomposition studies of a new, gem-dinitroalkyl nitramine 1,3,3-trinitroazetidine (TNAZ). Defence Sci J 46(5):361–369
18. Ma H, Feng X, Zhu T, Miao C, Ma Y, Feng M (2012) Research progress in high energy density material 1,3,3-trinitroazetidine. Chem Propell Ploym Mater 10(4):20–24
19. Zhang C (2009) Review of the establishment of nitro group charge method and its applications. J Hazard Mater 161(1):21–28
20. Katritzky A, Sommen G, Gromova A, Witek R, Steel P, Damavarapu R (2005) Synthetic routes towards tetrazolium and triazolium dinitromethylides. Chem Heterocycl Com 41(1):111–118
21. Göbel M, Klapötke TM (2009) Development and testing of energetic materials: the concept of high densities based on the trinitroethyl functionality. Adv Funct Mater 19(3):347–365
22. Puchala A, Belaj F, Bergman J, Kappe CO (2001) On the reaction of 3, 4-dihydropyrimidones with nitric acid. Preparation and X-ray structure analysis of a stable nitrolic acid. J Heterocyclic Chem 38(6):1345–1352
23. Bellamy AJ, Latypov NV, Goede P (2002) Transamination reactions of 1,1-diamino-2,2-dinitroethene (FOX-7). J Chem Res 2002(6):257–257
24. Zeng Z, Gao H, Twamley B, Shreeve JM (2007) Energetic mono and dibasic 5-dinitromethyltetrazolates: synthesis, properties, and particle processing. J Mater Chem 17(36):3819–3826
25. Oh CH, Park DI, Ryu JH, Cho JH, Han J (2007) Syntheses and characterization of cyclopropane-fused hydrocarbons as new high energetic materials. B Korean Chem Soc 28(2):322
26. Bulusu S, Damavarapu R, Autera J, Behrens R Jr, Minier L, Villanueva J, Jayasuriya K, Axenrod T (1995) Thermal rearrangement of 1,4-dinitroimidazole to 2,4-dinitroimidazole: characterization and investigation of the mechanism by mass spectrometry and isotope labeling. J Phys Chem 99(14):5009–5015
27. Minier L, Behrens R, Bulusu S (1996) Mass spectra of 2,4-dinitroimidazole and its isotopomers using simultaneous thermogravimetric modulated beam mass spectrometry. J Mass Spectrom 31(1):25–30
28. Bracuti A (1995) Crystal structure of 2,4-dinitroimidazole (24DNI). J Chem Crystallogr 25(10):625–627
29. Cho SG, Park BS, Cho JR (1999) Theoretical studies on the structure of 1,2,4,5-tetranitroimidazole. Propell Explos Pyrot 24(6):343–348
30. Rice BM, Hare JJ (2002) A quantum mechanical investigation of the relation between impact sensitivity and the charge distribution in energetic molecules. J Phys Chem A 106(9):1770–1783
31. Cho JR, Kim KJ, Cho SG, Kim JK (2002) Synthesis and characterization of 1-methyl-2,4,5-trinitroimidazole (MTNI). J Heterocyclic Chem 39(1):141–148
32. Thottempudi V, Gao H, Shreeve JM (2011) Trinitromethyl-substituted 5-nitro-or 3-azo-1,2,4-triazoles: synthesis, characterization, and energetic properties. J Am Chem Soc 133(16):6464–6471
33. Frisch MJ, Trucks GW, Schlegel HB, Scuseria GE, Robb MA, Cheeseman JR, Montgomery JA, Vreven T, Kudin KN, Burant JC, Millam JM, Iyengar SS, Tomasi J, Barone V, Mennucci B, Cossi M, Scalmani G, Rega N, Petersson GA, Nakatsuji H, Hada M, Ehara M, Toyota K, Fukuda R, Hasegawa J, Ishida M, Nakajima T, Honda Y, Kitao O, Nakai H, Klene M, Li X, Knox JE, Hratchian HP, Cross JB, Bakken V, Adamo C, Jaramillo J, Gomperts R, Stratmann RE, Yazyev O, Austin AJ, Cammi R, Pomelli C, Ochterski JW, Ayala PY, Morokuma K, Voth GA, Salvador P, Dannenberg JJ, Zakrzewski VG, Dapprich S, Daniels AD, Strain MC, Farkas O, Malick DK, Rabuck AD, Raghavachari K, Foresman JB, Ortiz JV, Cui Q, Baboul AG, Clifford S, Cioslowski J, Stefanov BB, Liu G, Liashenko A, Piskorz P, Komaromi I, Martin RL, Fox DJ, Keith T, Al-Laham MA, Peng CY, Nanayakkara A, Challacombe M, Gill

PMW, Johnson B, Chen W, Wong MW, Gonzalez C, Pople JA (2004) Gaussian 03, revision C02. Gaussian, Inc., Wallingford
34. Benson SW (1976) Thermochemical kinetics: methods for the estimation of thermochemical data and rate parameters. Wiley, New York
35. Yao XQ, Hou XJ, Wu GS, Xu YY, Xiang HW, Jiao H, Li YW (2002) Estimation of CC bond dissociation enthalpies of large aromatic hydrocarbon compounds using DFT methods. J Phys Chem A 106(31): 7184–7189
36. Shao J, Cheng X, Yang X (2005) Density functional calculations of bond dissociation energies for removal of the nitrogen dioxide moiety in some nitroaromatic molecules. J Mol Struc-Theochem 755(1): 127–130
37. Fan XW, Ju XH, Xia QY, Xiao HM (2008) Strain energies of cubane derivatives with different substituent groups. J Hazard Mater 151(1): 255–260
38. Politzer P, Martinez J, Murray JS, Concha MC, Toro-Labbe A (2009) An electrostatic interaction correction for improved crystal density prediction. Mol Phys 107(19):2095–2101
39. Chase MW Jr (1998) NIST-JANAF thermochemical tables, 4th edn. J Phys Chem Ref Data Monogr 9:1–1951
40. Rice BM, Pai SV, Hare J (1999) Predicting heats of formation of energetic materials using quantum mechanical calculations. Combust Flame 118(3):445–458
41. Politzer P, Lane P, Murray JS (2011) Computational characterization of a potential energetic compound: 1,3,5,7-tetranitro-2,4,6,8-tetraazacubane. Cent Eur J Energetic Mater 8(1):39–52
42. Kamlet MJ, Jacobs SJ (1986) A simple method for calculating detonation properties of CHNO explosives. J Chem Phys 48:23–25
43. Politzer P, Murray JS, Grice ME, Sjoberg P (eds) (1991) Computer-aided design of monopropellants. In: Olah GA, Squire DR (eds) Chemistry of energetic materials. Academic, San Diego
44. Benson SW (ed) (1976) Thermochemical kinetics, 2nd edn. Wiley, New York
45. Oxley JC, Smith JL, Ye H, McKenney RL, Bolduc PR (1995) Thermal stability studies on a homologous series of nitroarenes. J Phys Chem 99(23):9593–9602
46. Tsang W, Robaugh D, Mallard WG (1986) Single-pulse shock-tube studies on C–NO_2 bond cleavage during the decomposition of some nitro aromatic compounds. J Phys Chem 90(22):5968–5973
47. Li J (2010) Relationships for the impact sensitivities of energetic C-nitro compounds based on bond dissociation energy. J Phys Chem B 114(6):2198–2202
48. Song X, Cheng X, Yang X, Li D, Linghu R (2008) Correlation between the bond dissociation energies and impact sensitivities in nitramine and polynitro benzoate molecules with polynitro alkyl groupings. J Hazard Mater 150(2):317–321
49. Chen G, Shi WY, Xia MZ, Lei W, Wang FY, Gong XD (2014) Theoretical study of solvent effects on RDX crystal quality and sensitivity using an implicit solvation model. J Mol Model 20(7):1–9
50. Murray JS, Concha MC, Politzer P (2009) Links between surface electrostatic potentials of energetic molecules, impact sensitivities and C–NO_2/N–NO_2 bond dissociation energies. Mol Phys 107(1): 89–97
51. Politzer P, Murray JS (2014) Detonation performance and sensitivity: a quest for balance. Adv Quantum Chem 69:1–30
52. Ju XH, Wang ZY, Yan XF, Xiao HM (2007) Density functional theory studies on dioxygen difluoride and other fluorine/oxygen binary compounds: availability and shortcoming. J Mol Struc-Theochem 804(1):95–100
53. Zhou Z, Parr RG, Garst JF (1988) Absolute hardness as a measure of aromaticity. Tetrahedron Lett 29(38):4843–4846
54. Lu T, Chen F (2012) Multiwfn: a multifunctional wavefunction analyzer. J Comput Chem 33(5):580–592
55. Zhang XL, Gong XD (2014) Theoretical studies on the stability, detonation performance and possibility of synthesis of the nitro derivatives of epoxyethane. J Mol Model 20(8):1–11
56. Zhang XL, Yang JQ, Wang TY, Gong XD (2014) A theoretical study on the stability and etonation performance of 2,2,3,3-tetranitroaziridine (TNAD). J Phys Org Chem
57. Li ZX (2005) Study on the performance of several kinds of furazan energetic derivatives. Energ Mater 13(2):90–93
58. Chase MW, Force JANA (eds) (1998) NIST-JANAF thermochemical tables. American Chemical Society, Washington, DC